Structural and Adsorptive Characteristics of 2D Multilayer Nanoflakes of NiCo Phosphates for Chromium(VI) Removal: Experimental and Monte Carlo Simulations

Mai M. Khalaf,* Mohamed Gouda,* Kamal Shalabi, Saad Shaaban, and Hany M. Abd El-Lateef*

ACCESS | Metrics & More | Article Recommendations

ABSTRACT: Metal phosphates are efficient adsorbent materials for heavy elements present in industrial effluents because of their promising properties. Hexachromium ions are among the most dangerous contaminants owing to their harmful properties and non-degradability. Accordingly, the present work offers a simplified study of the preparation of bimetallic phosphate materials from nickel cobalt phosphate (NiCo-Ph) based on the sol−gel method in an equimolar ratio. Characterization of the bulk, crystal phase, texture profile, and nanosize of NiCo-Ph was carried out using various techniques such as Fourier transform infrared spectroscopy, X-ray diffraction, X-ray photoelectron spectroscopy, nitrogen adsorption−desorption isotherm measurements, field emission scanning electron microscopy, transmission electron microscopy, and Raman spectroscopy. In this regard, the adsorption performance of NiCo-Ph was exemplified through six batch experiments, elucidating the impacts of the sorbent dose, initial concentration of pollutants, sorption time, temperature, pH, and shaking rate. According to UV/vis spectrophotometry measurements and their related calculations of NiCo-Ph, the maximum removal efficiency (RE %) of 92% and adsorption capacity (q_m) of 37 mg/g were achieved at pH = 6, a dose of 5.0 g/L, 100 mg/L of [Cr(VI)], 300 rpm, adsorption time of 60 min, and 298 K. Monte Carlo simulations were also carried out to correlate the experimental data with theoretical calculations that provided a higher negative value (-911.62 kcal mol^{-1}) for the adsorption energy of Cr(VI) in acidic medium. The adsorbent NiCo-Ph prepared by this direct method is therefore recommended for the quantification of Cr(VI) under slightly acidic solutions and at room temperature, which can maintain its efficiency even up to six cycles.
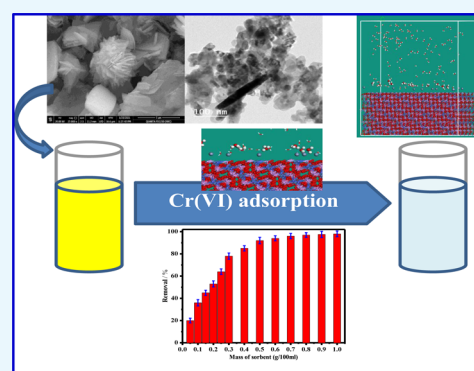
1. INTRODUCTION

One of the common toxic contaminants is heavy metals. They are not only non-biodegradable but also toxic due to their bioaccumulation in living cells. Among the documented toxic elements, Cr, As, Cd, Pb, Ni, Cu, Zn, and Hg[1] are not only dangerous for human health but also affect aquatic and environmental ecosystems. Consequently, it is necessary to purify the polluted waters from these heavy metals before being discharged into water bodies. Accordingly, several approaches were investigated for the removal of heavy metals including chemical precipitation,[2] electrodialysis,[3] electrocoagulation,[4] membrane filtration,[5] adsorption,[6] and photocatalysis.[7] Recently, adsorption has been a significant interest area with a special focus on recognizing low-cost adsorbents.[8−10]

Chromium exists in the environment generally in hexavalent and trivalent forms. Chromium in the hexavalent form is very poisonous and is located in the first assembly of carcinogenic materials. Chromium is one of the most commonly used heavy metals in different industrial applications such as dyeing, electroplating, tannery, and fertilizer production. When the

polluted water of these manufacturing industries enters the environment, the Cr metal spreads through the environment.[11] The U.S. Environmental Protection Agency has stated hexavalent chromium as one of the dangerous toxic contaminants, even in very low doses. Extreme chromium consumption by humans leads to renal and hepatic injury, gastrointestinal irritation, capillary damage, and central nervous system disorders. Chromium could lead to cancer of the digestive tract and lungs.[5] In wastewaters, Cr(VI) is predominantly present in the form of extremely soluble oxyanions, for instance, as bichromates, dichromates, and chromates. In order to decrease the severe harm caused by them, in particular, to ecology, it becomes the responsibility of these industries to diminish the Cr(VI) dose in their wastes to
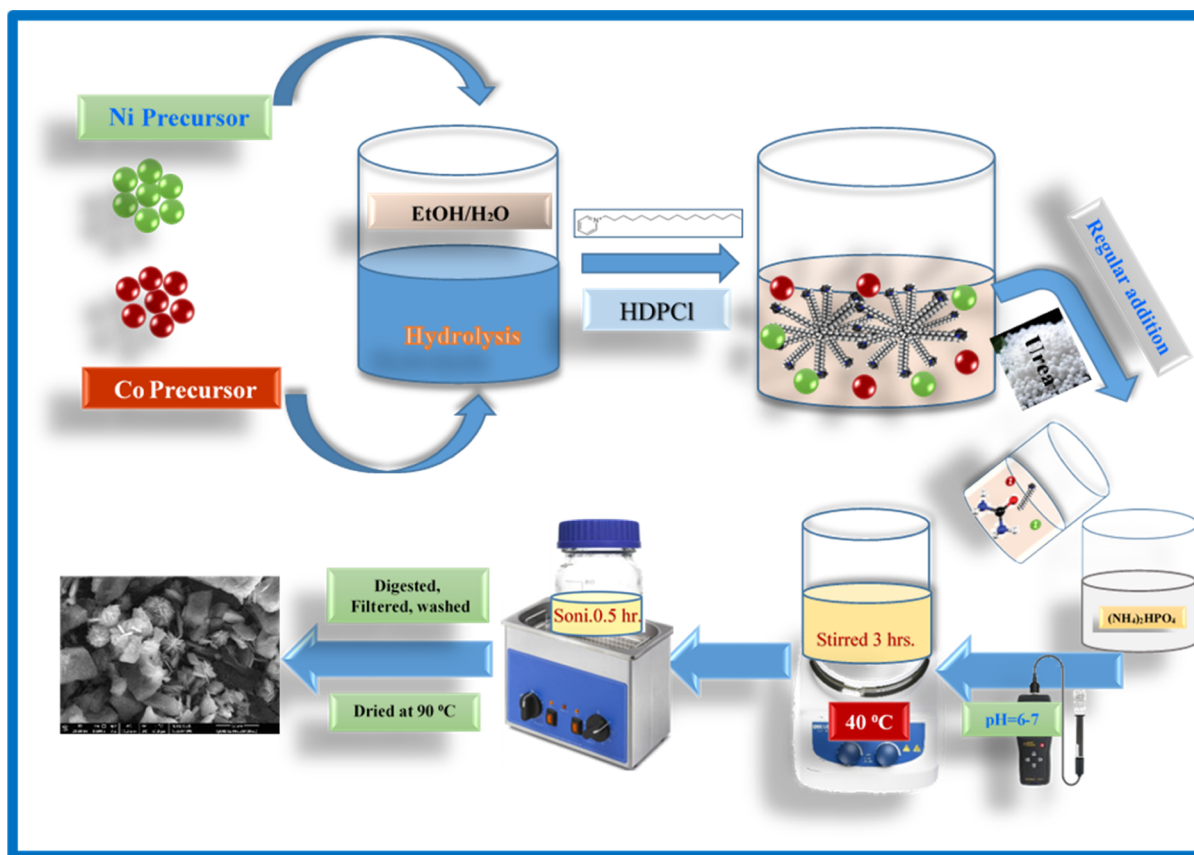
Figure 1. Scheme for the synthetic pathway of bimetallic NiCo-Ph.

a suitable level prior to releasing them into the environment. Also, the recovery of chromium present in wastewaters is an attractive choice for economic reasons.[4] The utilization of the above diverse approaches for removal of chromium appears to be restricted owing to the low removal capacity, comparatively high costs, release of wastes formed by treatment, the need for expending a great energy, the need for fixed system monitoring, production of toxic sludges, and generally the need for a high capital investment and high operating costs.[5−11]

Ultimately, the adsorption technique should be an efficient, facile, less-expensive, and eco-friendly approach. Additionally, it should be among the most operative and public-appropriate technology that is regularly utilized over other methods in the worldwide ecological protection zones.[12,13] Adsorption has numerous benefits over the orthodox approaches, which comprises sorbent reusability, low selectivity for precise metals, less operational cost, no chemical sludges, and a small operation time. Different scientists have investigated the efficiency of several other adsorbents for Cr(VI) removal from wastewater using fixed-bed and batch methods. Some of the adsorbents are *Leucaena leucocephala* seed shell-activated carbon,[14] activated carbon based on luffa sponge,[15] polyaniline doped with sulfuric acid,[16] magnetite nanoparticles,[17] and palm trunk charcoal.[18]

Eventually, these sorbents are non-eco-friendly and hardly reflected in their costs. On the other hand, bimetal phosphates are an alternative that are naturally approachable and have been extensively explored as adsorbents.[19] The well-structured morphology of metal phosphates has much advantage and displayed considerable success in numerous applications as

well as in technological advance.[20] They have been used in lithium batteries,[21] as catalysts for chemical conversion,[22] in electrocatalytic conversion processes,[23] and as supercapacitors.[24] Surprisingly, bimetal phosphate mesoporous adsorbents were scarcely reported in the literature.[20]

In this report, novel nanomesoporous NiCo-Ph was synthesized with a good surface area via a facile and cost-effective method. The introduced bimetal NiCo-Ph was characterized using field emission scanning electron microscopy (FE-SEM), transmission electron microscopy (TEM), X-ray diffraction (XRD), Fourier transform infrared (FTIR) spectroscopy, Raman spectroscopy, and X-ray photoelectron spectroscopy (XPS), and the pore size and BET surface area were also examined. Meanwhile, the nanomesoporous NiCo-Ph was utilized in the removal of hexavalent chromium ions from aqueous media. The batch technique was utilized; parameters including the contact time, pH, and initial chromium dose were investigated. Furthermore, Monte Carlo (MC) simulations were performed to confirm the experimental adsorption findings.

2. EXPERIMENTAL SECTION

2.1. Synthesis of NiCo-Ph. All the chemicals utilized in this approach were of analytical grade and used directly without any additional refinement. All the reagents were obtained from Sigma-Aldrich and Chemical Reagent Co., Ltd.

Figure 1 illustrates the sol−gel synthesis pathway to prepare the sample. In a typical blend of equimolar Ni and Co, precursors were hydrolyzed in a mixture of bidistilled water and EtOH (100:50). This is followed by adding a hexadecyl pyridinium chloride surfactant (HDPCl) with regular addition
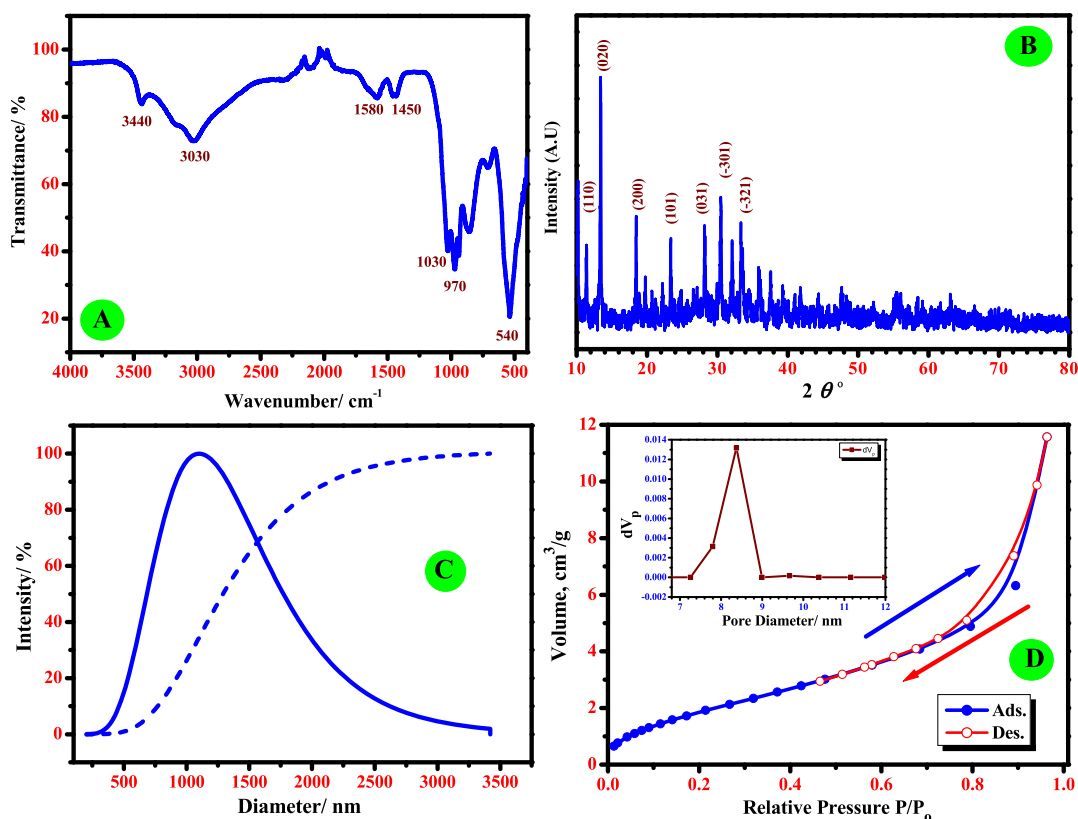
Figure 2. FT-IR spectrum (A); XRD diffractogram (B); DLS curve (C); and N_2 adsorption−desorption isotherm with its related pore diameter distribution of the investigated NiCo-Ph (D).

of urea to the previous blend under stirring for 15 min. Then, this mixture was dropwise transferred to an appropriate volume of ammonium monohydrogen phosphate $(NH_4)_2HPO_4$ by adjusting the pH to 6−7, and this mixture was subjected to stirring for further 3 h at a constant temperature of 40 °C. The resultant blend, which appeared as a sol, was sonicated for half an hour, then digested at room temperature to the next day, followed by filtration, washing, and drying at 90 °C for a day. The attained sample was abbreviated as NiCo-Ph, and it was characterized using various techniques.

2.2. Material Characterization. FTIR investigation was carried out in the range 400−4000 cm^{-1} using a Bruker FTIR spectrometer. Characterization of the bulk and the crystal phase of the sample as powder was done using an X-ray diffractometer at 2θ from 10 to 80°. XPS data were obtained as reported previously.[25] The specific surface area (S_{BET}) and pore diameter distribution were also determined via studying the nitrogen adsorption−desorption isotherms (Micromeritics ASAP2010) at 77 K using the Brunauer−Emmett−Teller method. The morphology of the powder sample was explored using a field emission scanning electron microscope equipped with an energy-dispersive X-ray spectrometer (JSM-5410 model JEOL, Japan). The particle profile and nanosize were estimated by TEM using a Jeol-1230 electron microscope working at 200 keV. Raman spectroscopy was utilized to study the stability of the chemical structure of the prepared adsorbent using a Raman spectrometer (Horiba Scientific, SUA) before and after the adsorption of Cr(VI).

2.3. Batch Adsorption Experimentations. All experiments were performed in the 298−328 K temperature range. The adsorption tests were completed in batches. The

experiments of batch adsorption were accomplished by shaking 0.5 g of NiCo-Ph with 100 mL of chromium(VI) solutions (5.0 g/L). The bottles were covered and stirred in a shaking water bath (THERMOLAB) at an agitated speed of 200−400 rpm. The concentration of chromium(VI) in the experimental medium was spectrophotometrically measured using a UV/vis spectrophotometer (model Shimadzu UV-1800 —Japan) in the wavelength range from 180 to 800 nm and in a 1.0 cm quartz cell. After the adsorption experiment, the absorbance values were measured at λ_{max} = 360.0 nm. All the tests were repeated three times, and the average of the results was recorded. The standard deviation ($\pm$SD) was calculated between 2.0 and 4.0% for all experiments. The influence of the NiCo-Ph sorbent mass (0.05−1.0 g/100 mL) on Cr(VI) removal was examined. The influence of the contact time on Cr(VI) adsorption was investigated from 0 to 200.0 min. The pH values of the tested experiments were adjusted from 1.0 to 8.0 using 0.1 M KOH or 0.01 M HNO$_3$. The removal efficacy (RE/%) of Cr(VI) and the amount of adsorbed Cr(VI) Q_e (mg/g) at equilibrium were calculated using the following equations

$$RE/\% = \left(\frac{C_i - C_e}{C_i}\right) \times 100 \tag{1}$$

$$Q_e = \left(\frac{C_i - C_e}{W}\right) \times V \tag{2}$$

where W (g) represents the sorbent weight, V (L) symbolizes the solution volume, And C_e and C_i (mg/L) are the equilibrium and initial Cr(VI) concentrations, respectively.
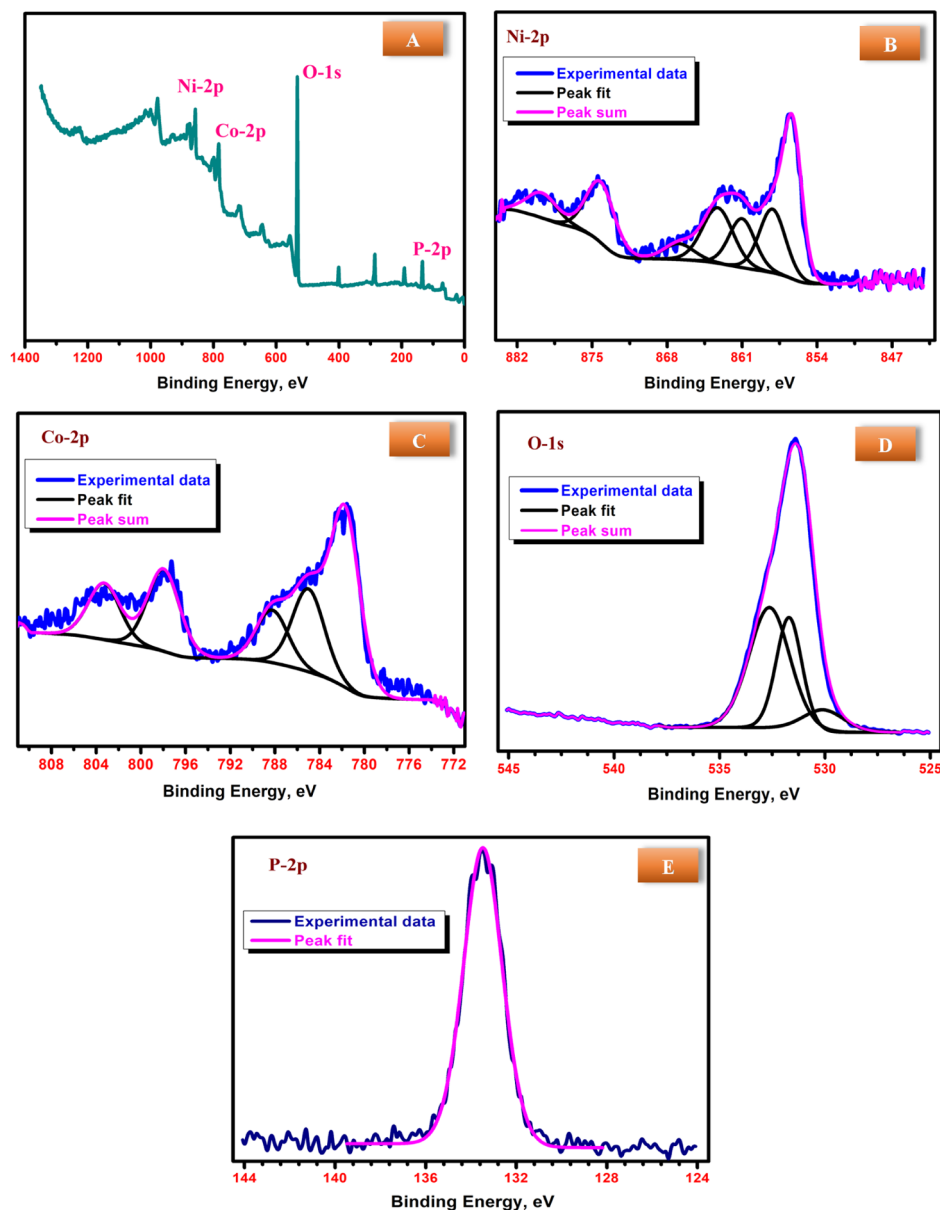
Figure 3. Full XPS analyses of the introduced NiCo-Ph sample: (A) full, (B) Ni 2p, (C) Co 2p, (D) O 1s, and (E) P 2p spectra.

2.4. MC Simulations. MC simulations have been accomplished utilizing the adsorption locator module in Materials Studio software V.7.0 from Accelrys Inc. USA. The adsorption locator discloses the appropriate adsorption arrangements of Cr(VI) ions with Monte Carlo (MC) searches on NiCo-Ph.[26] The adsorption of Cr(VI) ions in acidic (hydronium ions + water molecules), basic (hydroxide ions + water molecules), and neutral (water molecules only) media and on the surface of NiCo-Ph was achieved in a simulation box (32.27 Å × 32.27 Å × 50.18 Å) with periodic boundary tuning. The Forcite classical simulation engine was employed to improve the energy of Cr(VI) ions.[27] Also, the specifics of computational calculations were illustrated in our former published research.[27,28]

3. RESULTS AND DISCUSSION

3.1. Material Characterization. Figure 2A depicts the FTIR spectrum of the NiCo-Ph sample. The bands in the region of 3440−3030 cm^{-1} show the vibrational mode of crystalline water. A wideband at 3440−3250 cm^{-1} is due to the interference of OH groups in adsorbed water and the OH groups in ammonium ions.[29] Correspondingly, the bands of 1580 and 1450 cm^{-1} are ascribed to the bending mode of H$_2$O. A group of small bands lying in the region of 1030−970 and 860 cm^{-1} is assigned to the vibrational mode of the anion of PO$_4^{3-}$ as symmetric and asymmetric O−P−O, respectively. In the low-frequency region, a sharp band of bending of P−O is detected at 540 cm^{-1}.

Figure 2B illustrates the XRD pattern of the studied sample, pointing out the effective sol−gel route in synthesizing the bimetal Ni and Co phosphates. The pattern shows piercing diffraction peaks at 2θ = 11.48, 13.40, 18.47, 23.30, 28.23, 30.36, and 33.35°. Furthermore, the predominant (*hkl*) planes of (110), (020), (200), (101), (031), ($\bar{3}$01), and ($\bar{3}$21), respectively, are consistent with the described phase of the monoclinic hydrated nickel phosphate and monoclinic hydrated cobalt phosphate (XRD cards 00-033-0951 and 00-041-0375).[30] The grain size was assessed to be 66 nm using

the full width at half-maximum (fwhm) value and the Debye−Scherrer equation. This result is in good agreement with the particle size, as estimated by SEM studies.

To clarify the distribution of the hydrodynamic size of the NiCo-Ph sample, Figure 2C displays its dynamic light scattering (DLS) distribution in the investigated medium of Cr(VI). DLS measurement displays a broad size distribution of 333−2350 nm and is maximized at 1100 nm. On the other hand, this hydrodynamic size is greater than the particle size distribution illustrated by SEM and TEM methods, which is due to the electric double layer on the particle interface.

The nitrogen adsorption/desorption isotherm plot (Figure 2D) displays the isotherm type, which is indexed to the type IV isotherm and characterized to be mesoporous nanomaterials. The specific surface area S_{BET} and pore width distributions were estimated to be 8 m^2/g and 8.4 nm, respectively. This good value in terms of pore width distribution that is in the mesoporous range is the reason behind the efficiency of the NiCo-Ph sample in Cr(VI) removal. This in turn is needed to achieve a reasonable Cr(VI) adsorption capacity in a quite short contact time.

XPS investigation of the NiCo-Ph sample was carried out to show the valence or electronic surface states of the contents. The XPS spectra (Figure 3A) and their data (Table 1) show

Table 1. XPS Investigation of the Prepared NiCo-Ph Sample

peak	start BE	peak BE	end BE	height CPS	fwhm eV	atomic %
O 1s	535.64	530.56	529.1	57 052.2	3.54	49.08
Ni 2p	867.51	859.89	852.09	13 072.53	2.55	3.39
Co 2p	811.08	784.08	778.07	14 418.05	6.69	7.39
P 2p	140.48	136.33	129.08	7562.43	3.54	11.44

good agreement with the XRD data. Figure 3A shows all regions of the XPS spectrum that is characterized for Ni 2p (859.8 eV), Co 2p (784.1 eV), O 1s (530.6 eV), and P 2p (136.3 eV). The short XPS spectrum points to the oxidation states of NiCo-Ph as Ni (II), PO_4^{3-}, and Co^{3+}. Minutely, the high-resolution XPS spectrum (Figure 3B) in the range of binding energy of Ni 2p displays typical peaks at 879.8 and 856.4 eV as well as satellite peaks, which are attributed to Ni $2p_{1/2}$ and Ni $2p_{3/2}$, respectively,[31] that confirmed the presence of Ni as Ni^{2+} in the prepared NiCo-Ph sample. Correspondingly, peaks at 798 and 782 eV (Figure 3C) are attributed to Co^{3+} and Co^{2+} ions and are distinguished as the binding energy peaks of Co $2p_{1/2}$ and Co $2p_{3/2}$, respectively.[32] The two main peaks go along with two satellite peaks centered at 788.3 and 784.88 eV due to the high spin of the Co^{2+} ion. The peak at 782 eV was due to the Co oxidation state being linked with Co−PO_x, which is probably caused by the surface oxidation.[33−35] The O 1s spectrum is shown in Figure 3D, the deconvoluted or fitted O 1s peaks at 530.1, 531.7, and 532.6 eV are attributed to M−O or hydroxyl groups. Figure 3E represents a peak at 134.2 eV, which is attributed to P−O of (PO_4).[36]

SEM micrographs at different magnifications are depicted in Figure 4A,B. As is clearly shown, the examined sample showed a nanoflake morphology in two dimensions, which accumulated above each other forming a multilayer with a nanoflower shape. The lengths of nanoflakes range from 100 to 200 nm. Analysis of SEM results was done with ImageJ software. The histogram of nanoparticles (Figure 4F) shows a reasonable size

distribution from 3 to 40 nm with a mean size distribution of 20 ± 2 nm.

A further study of the morphology and topology of the NiCo-Ph sample was also carried out using TEM (Figure 4C,D). Typically, the profile of the sample, where the nanoflakes appear on one side and full nanoflakes mixed with semispherical particles with diameters ranging from 20 to 80 nm. These results are in full agreement with those obtained using SEM.

The corresponding SAED image is presented in Figure 4E, which illustrates all rings of different planes with a lattice gap (d-spacing) of 6.5 Å matching with the high relative intensity (100%) of the (020) plane of Co 2p and Ni 2p, which is proportionate to the XRD findings.

3.2. Adsorption Study. Toward estimating the ability of the prepared bimetal phosphate NiCo-Ph as a potential adsorbent for Cr(VI) ions from aqueous phases, six analogous control experiments were carried out to study and identify the optimum parameters required for the adsorption of chromium ions using the adsorbent prepared.

At first, Figure 5 depicts the variations between the absorption spectra at time intervals ranging from 0 to 100 min for 100 mL sample of Cr(VI) ions (100 mg/L) containing 0.5 g/100 mL of NiCo-Ph at 298 K; there are two distinct peaks, an obvious sharp peak at λ = 360 nm and a slight broad peak at 425 nm. As noticeable, there is a diminution in the intensity of spectral curves with increasing time, where the sharp peak at 360 nm slightly faded after 100 min of contact time. The difference in intensities of the UV−vis spectra confirms the superior performance of the NiCo-Ph adsorbent, which is due to the low concentrations of Cr(VI) species.

Therefore, Figure 6A shows the effect of the sorbent dose within the range of 0.1−1 g/100 mL in a control experiment at pH = 6, with an initial concentration of Cr(VI) of 100 mg/L, a T of 298 K, and a contact time of 60 min. The removal efficiency (%) distinctly increases with the increase of the adsorbent weight and reaches 92% by consuming 5.0 g/L of the examined sorbent. After that, the upturn is slight and does not clearly intrude on the efficiency of the adsorbent. The enhancement of the removal efficiency by increasing the adsorbent dose can be attributed to the availability of the free active sites on the surface of our adsorbent. The binding may be due to the electrostatic attraction between the charged positive surfaces of NiCo-Ph and the anionic chemistry of solutions of chromium ions in an adsorption process at pH = 6. The optimum mass of the sorbent was identified to be 5.0 g/L of Cr(VI) ions (100 mg/L).

Another control experiment disclosed the sufficient contact time for the adsorption of Cr(VI) ions on the surface of the bimetallic phosphate sample (Figure 6B). This control experiment was carried out at pH = 6, with the adsorbent dose of 5.0 g/L, and [Cr(VI)] of 100 mg/L at a contact time interval of 15−200 min. This behavior facilitated enhancing the removal efficiency of up to 92% at 60 min accompanied by a flat plateau even after undergoing further sorption. This asserted the consumption of free active sites accessible for the Cr(VI) sorption. The initial Cr(VI) dose is shown in Figure 6C for another control experiment using an adsorbent dose of 5.0 g/L, pH = 6, a sorption time of 60 min, and a concentration range of 20−250 mg/L. As detectable from the Cr(VI) dose graph, there is a slight change observed in the Cr(VI) sorption on the NiCo-Ph surface upon increasing the Cr(VI) dose up to 250 mg/L, especially after 100 mg/L, which
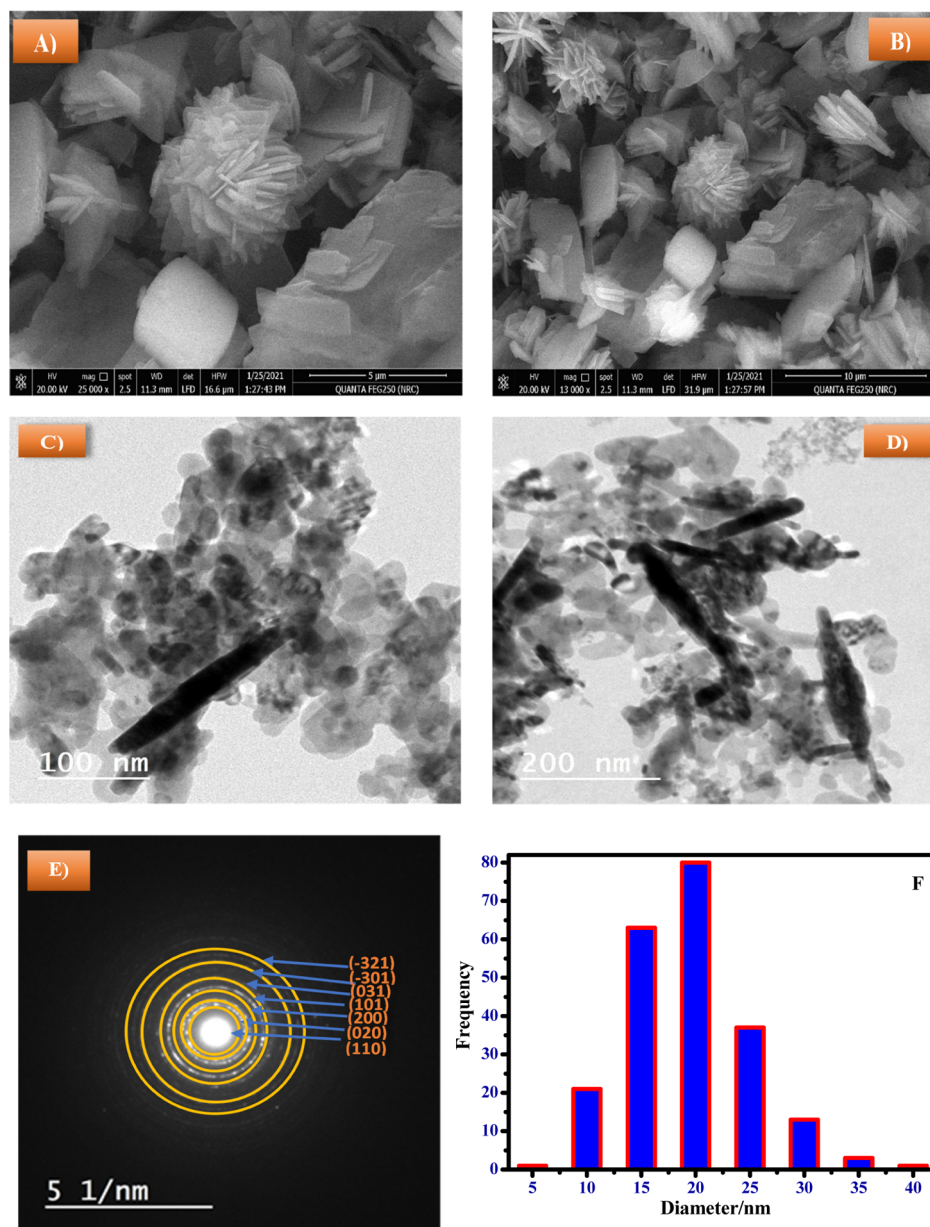
Figure 4. FE-SEM micrographs at two different magnifications (A,B); TEM micrographs at different magnifications (C,D); SAED image (E); and histogram of the nanoparticle diameter (F) of the investigated NiCo-Ph sample.

corresponds to the removal of 92%. This reasonable removal % value of 92% is sufficiently obtainable for a high Cr(VI) dose of 100 mg/L. Furthermore, the removal % decreased from 92 to 75% with increasing Cr(VI) concentrations, which caused the active centers of the used adsorbent to become saturated and clogged.

Figure 6D exemplifies the influence of the shaking speed on Cr(VI) sorption, which was scrutinized under a controlled experiment at pH = 6, 25 °C, 0.5 g NiCo-Ph/100 mL, an adsorption time of 60 min, and [Cr(VI)] = 100 mg/L, within speed limits of 200−400 rpm. To clarify the role of the shaking rate, the shaking rate was increased, and a drastic change in the removal % value was noted from 75% at 200 rpm until reaching 97.5% at 300 rpm. However, increase of the shaking rate to higher than 300 rpm has no significant change in the removal rate, declaring the adequacy of this speed rate (300 rpm) for the outer transfer from the bulk solution of Cr(VI)

ions to the frontier surface of the used adsorbent. Previous analogous effects reported the adsorption of Cr(VI) solutions.[37,38]

Another control experiment was also conducted for studying the impact of alteration of temperature. The test was conducted in the temperature range of 298, 308, 318, and 328 K, keeping the other control parameters of pH = 6, 0.5 g NiCo-Ph/100 mL, adsorption time of 60 min, and [Cr(VI)] = 100 mg/L the same (Figure 7A). Unexpectedly, the increase in temperature causes a slight diminution in the rate of Cr(VI) removal (%) from 97% at 298 K to 85% at 328 K. This outcome may be elaborated in terms of the nature of the pores of the investigated adsorbent. In addition, a competitive desorption process has occurred instead of the adsorption process due to the high thermal energy. This distinguishes our absorbent NiCo-Ph for its efficiency under ambient conditions.
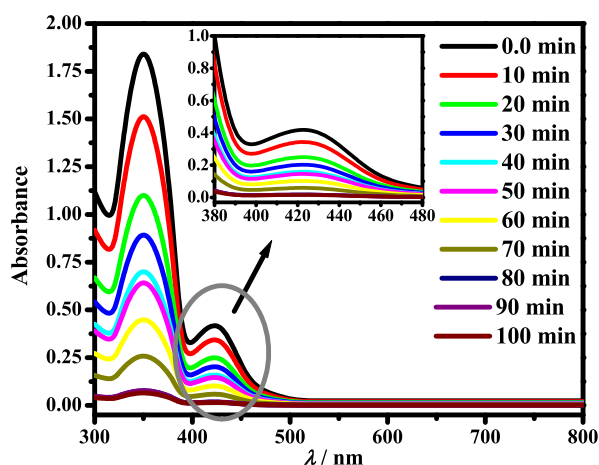
Figure 5. UV−vis spectra of chromium(VI) in the presence of 0.5 g/100 mL NiCo-Ph at different times (100 mL of 100 mg/L Cr(VI) at 25 °C).

A comparable approach also illuminated this effect for the adsorptive removal of Cr(VI) from an aqueous solution.[39]

Figure 7B depicts the effect of varying pH from 4 to 9 on the removal rate %, with the same control parameters of 0.5 g NiCo-Ph/100 mL, an adsorption time of 60 min, 25 °C, and [Cr(VI)] = 100 mg/L. As is clearly shown, an increase in the removal rate % to 92% has been observed upon increasing the pH value to reach a maximum of 6.0. Then, a decline in the

removal % value was observed at pH values >6, and the removal % was as low as 30% at pH = 9.

From these insights, it can be said that the adsorption of hexavalent chromium ions is fundamentally contingent on the pH value of a solution. This can be due to the active groups on the adsorbent surface as well as the structure or valence of chromium ions present in the solution. Cr(VI) removal using NiCo-Ph as an adsorbent is preferred at slightly acidic pH. Previous contributions reported that at acidic pH values, the metal ions in bimetal phosphates exist as positive ions until pH 6, which are then converted to negatively charged metal phosphate ions at pH greater than 7.[40] Therefore, as described by XPS outcomes, bimetal phosphates (NiCo-Ph) are present in Ni^{2+} and Co^{3+} species. Besides, the prevailing ionic forms of Cr ions in the aqueous solution are $HCr_2O_7^-$ or $Cr_2O_7^{2-}$ at slightly acidic pH.[41] Under these conditions, an electrostatic attraction arises between the anionic species of chromium and the positively charged surface of NiCo-Ph through an anionic adsorption process, which is prominently improved. While with the increment of pH values, the surface layer of the adsorbent NiCo-Ph became negatively charged as MPO_4^-. In addition, CrO_4^{2-} and OH^- ions were initiated in an intense rivalry, hence a mutual repulsion takes place resulting in poor sorption of Cr(VI). Moreover, this effect can be elucidated in terms of pH-response characteristics, which enables the examined sorbent to behave as a hydrophilic adsorbent under acidic conditions and as an amphiphilic adsorbent under slightly neutral conditions. This can be attributed to the
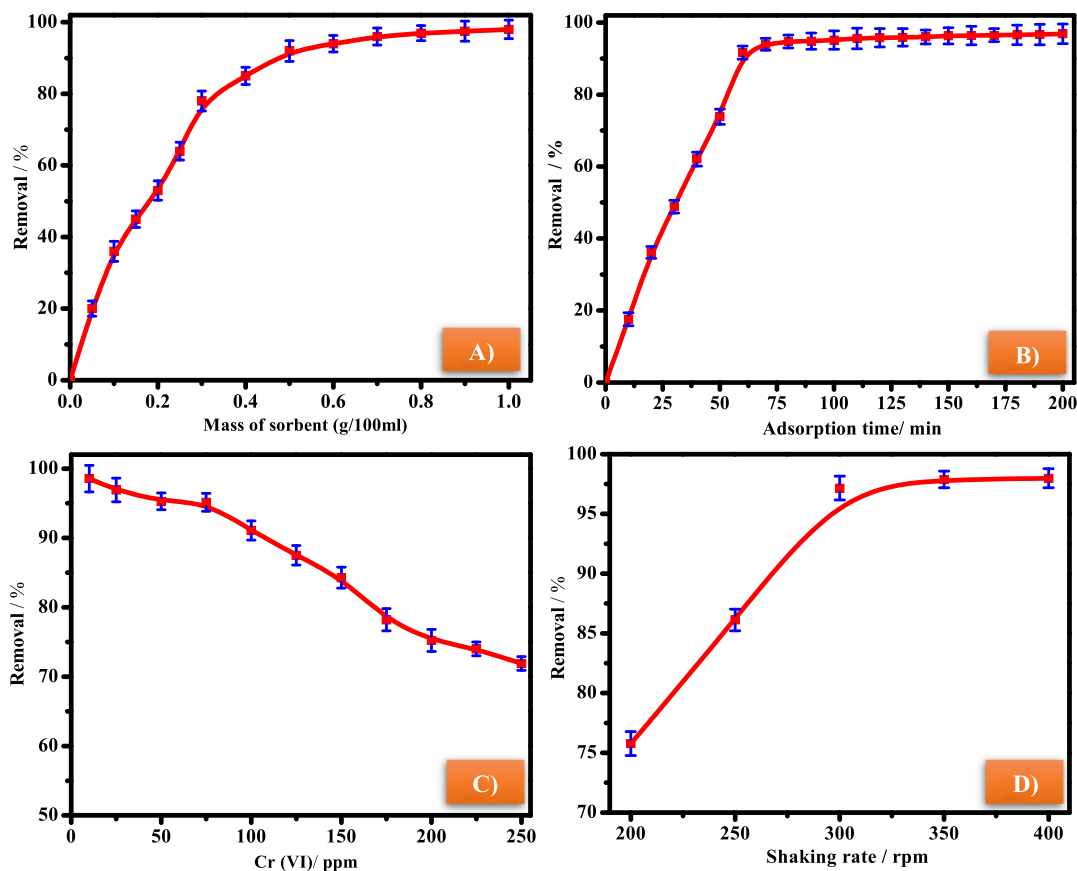

Figure 6. Effect of the mass of the sorbent (100 mL of 100 mg/L Cr(VI)) (A); adsorption time (100 mL of 100 mg/L Cr(VI), 0.5 g/100 mL NiCo-Ph) (B); initial Cr(VI) dose (0.5 g NiCo-Ph) (C); shaking speed for 100 mL of 100 mg/L Cr(VI), 0.5 g/100 mL NiCo-Ph; and contact time of 60 min (D) on the adsorption (removal) of Cr(VI) by NiCo-Ph; pH = 6, at 25 °C.
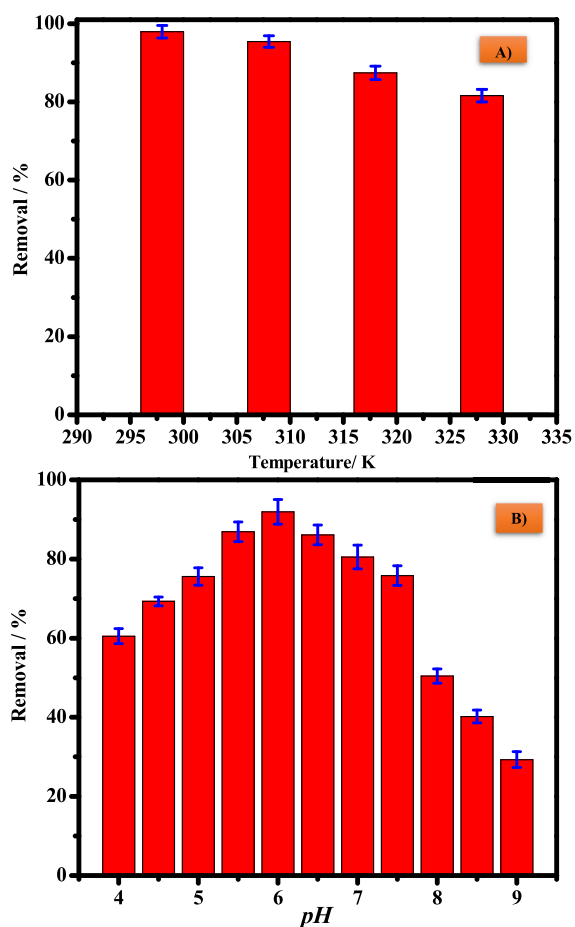
Figure 7. Effect of the temperature (pH = 6) (A) and pH (B) on the adsorption (removal) of Cr(VI) by NiCoPh; 0.5 g/100 mL of NiCoPh, 100 mL of 100 mg/L Cr(IV), 0.5 g/100 mL NiCo-Ph, at a contact time of 60 min.
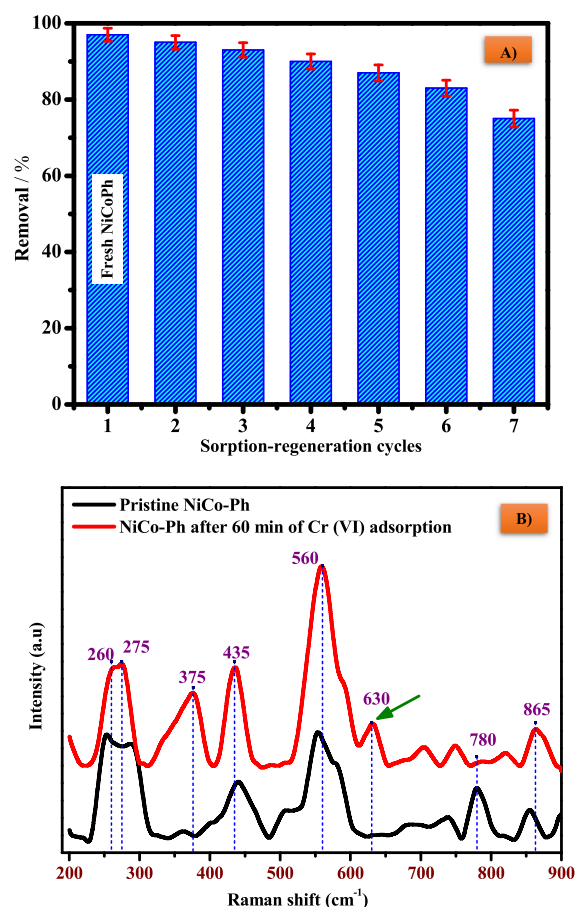

Figure 8. Regeneration of the NiCo-Ph sorbent (100 mL of 100 mg/L Cr(VI), 0.5 g sorbent/100 mL and 25 °C) (A) and Raman spectra of pristine NiCo-Ph before Cr(VI) removal and of NiCo-Ph after 60 min of Cr(VI) adsorption (B).

use of HDPCl as a cationic surfactant in the preparation route of the synthesized adsorbent. The amine surfactants have higher amphiphilic property at low pH values once the NH_2 group is protonated. Consequently, these amine groups in the used surfactant likely act as pH-responsive amphiphiles.[42] Thus, they can competently enhance the degradation of adsorbed Cr(VI) ions with outstanding recyclability; a similar previous study was reported by Shi et al.[43] It can also be interpreted in terms of adsorption energy and its correlation with the removal ability of Cr(VI), as will be elaborated in the following section of MC Simulations.

Figure 8A discloses the regeneration of the NiCo-Ph sorbent through seven repetitive cycles under optimum conditions, which were selected as illustrated previously (100 mL of 100 mg/L Cr(VI), 5.0 g/L sorbent, pH = 6, and 25 °C). The probability of the used adsorbent due to its activity preserved the outstanding adsorption behavior over several cycles. The outcomes revealed a minor lessening in the removal efficiency of hexachromium ions from 96% up to ~80% after seven cycles. Figure 8B shows the Raman spectra of NiCo-Ph before and after 60 min of Cr(VI) removal. This is to approve the establishment of NiCo-Ph and its stabilization even after 60 min as optimum adsorption time for Cr(VI) removal. A pronounced sharp peak was observed at 560 cm^{-1}, which is attributed to ν antisymmetric bending vibrations of the phosphate bond P−O−P.[44] A slight shift of the peak at 780

cm^{-1} (before the adsorption process) at a lower wavenumber was noted that may be pronounced for phosphate network modifiers or a system of transition metals doped with P_2O_5.[45] Moreover, this lower shift was also observed at 865 cm^{-1} for the NiCo-Ph sample after the adsorption process at 900 cm^{-1}, which is ascribed to the vibrational stretching terminal O atom containing the PO_4 group,[44] thus confirming the construction of a hydrated Ni−Co phosphate phase. The spectra display bands at 435 and 445 cm^{-1} corresponding to the stretching vibrations of Ni−O.[36] Furthermore, the pronounced peaks at 350−375 cm^{-1} were assigned to the bending vibrations of O−Co−O. The lattice vibration peaks of specific clusters of the samples are observed below 300 cm^{-1} at 260 and 275 cm^{-1}.[46] Furthermore, the sample of NiCo-Ph after association with chromium(VI) disclosed a typical peak in the range of 630 cm^{-1} which is associated with the existence of Cr(III), declaring the efficiency of the prepared NiCo-Ph in the reduction of Cr(VI) to Cr(III) ions and thereby its potential for remediation of water from Cr(VI) ions.[47,48]

3.3. Adsorption Isotherm Considerations. In order to estimate the adsorption efficiency of NiCo-Ph nanoflakes, chromium(VI) adsorption onto 0.5 g nano-NiCo-Ph/100 mL Cr(VI) at equilibrium is investigated using the models of Langmuir and Freundlich isotherms.[49] The Freundlich model was commonly used to describe the inhomogeneity of the surface. The model of Langmuir assumes that adsorption takes place on the adsorbent's external interface. The Langmuir

model supposes the occurrence of construction of the sorbate molecules on the homogeneous interface of the sorbent. The Freundlich and Langmuir models were defined by the following equations[50]

Freundlich model $\qquad \log q_e = \dfrac{1}{n} \log C_e + \log K_f$ (3)

Langmuir model $\qquad \dfrac{1}{q_e} = \dfrac{1}{q_m K_L} \dfrac{1}{C_e} + \dfrac{1}{q_m}$ (4)

where C_e is the Cr(VI) equilibrium concentration in medium (mg/L), n is the Freundlich exponent interrelated to adsorption power, K_f represents the Freundlich constant (mg/g), $1/n$ characterizes the adsorption density, q_m represents the maximum adsorption efficacy (mg/g), K_L is the Langmuir constant (L/mg), and q_e symbolizes the adsorption effectiveness at equilibrium (mg/g). The above-revealed factors can be obtained from the relation of C_e/q_e versus C_e and $\log q_e$ versus $\log C_e$ plots. The value of n was found to be 2.21 (greater than 1), which designates that the adsorption process has promising ability. The linear plots of Langmuir and Freundlich isotherm models for Cr(VI) at pH = 6 and a sorbent weight of 0.5 g/100 mL Cr(VI) are presented in Figure 9A,B. The computed parameters of the investigated adsorption models are recorded in Table 2. Based on the correlation coefficient values (R_2), the data fit well to the model of Langmuir ($R^2 = 0.986$) than to the Freundlich model ($R^2 = 0.965$). The characteristics and feasibility of the

Figure 9. Linear diagrams of (A) Langmuir model and (B) Freundlich model for Cr(VI); pH = 6 and sorbent weight = 0.5 g/ 100 mL Cr(VI).

Table 2. Adsorption Isotherm Parameters for Cr(VI) Adsorption on the 0.5 g/100 mL NiCO-Ph Sample

model	Langmuir			Freundlich		
parameters	q_{max} (mg/g)	K_L (L/mg)	R^2	K_f	n	R^2
values	35.7	0.411	0.986	5.81	2.20	0.965

Langmuir model according to the factor of dimensional separation, R_L, is given using the following formula[51]

$$R_L = \frac{1}{K_L C_i + 1}$$

(5)

where C_i is the initial concentration of Cr(VI). The values of R_L confirm if the adsorption is promising ($0 < R_L < 1$), irreversible ($R_L = 0$), linear ($R_L = 1$), or unfavorable ($R_L > 1$). The R_L value for the investigated sorbent NiCo-Ph nanoflakes was found to be 0.023 (in the range of $0 < R_L < 1$). This value specifies a suitable adsorption isotherm type of Cr(VI) ions onto the NiCo-Ph surface in the examined concentration range. The n value changes with the sorbent heterogeneity and indicates the favorability of the adsorption route. The n value should be $10 < n > 1$ under promising adsorption conditions. The value of n in the present report was found to be 2.20, which displays that the Cr(VI) sorption onto NiCo-Ph nanoflakes is favorable.

3.4. MC Simulations. MC simulations were carried out to study the adsorption between the Cr(VI) ions and the NiCo-Ph surface. Figure 10 therefore shows the highest proper adsorption arrangements for the Cr(VI) ions on the NiCo-Ph surface achieved using the adsorption locator module.[52] Furthermore, the attained outcomes from the MC simulations are shown in Table 3 such as the adsorption energy for relaxed adsorbate molecules, rigid adsorption energy for unrelaxed adsorbate molecules, and deformation energy for relaxed adsorbate molecules.[53] Table 3 divulges that Cr(VI) (-911.62 kcal mol^{-1}) has a higher negative value of adsorption energy in acidic medium in comparison with the value of Cr (VI) in basic or neutral medium, which confirms the powerful adsorption of Cr(VI) ions on the NiCo-Ph surface in acidic medium. Additionally, the values listed in Table 3 manifest that the adsorption energy values of Cr(VI) in acidic medium pre- and postgeometry optimization steps (i.e., unrelaxed and relaxed values of -822.88 and -88.7379 kcal mol^{-1}, respectively) are further negative than those in basic or neutral medium, asserting the higher adsorption of Cr(VI) ions on the NiCo-Ph surface in acidic medium.

The adsorption energy of an adsorbate when one of the adsorbates has been omitted is elucidated through the dE_{ads}/dN_i values.[54] The dE_{ads}/dN_i values for Cr(VI) in acidic medium (-162.59 kcal mol^{-1}) are higher than those in basic or neutral medium, which declares the excellent adsorption of Cr(VI) ions on the NiCo-Ph surface in acidic medium. Moreover, the dE_{ads}/dN_i values of water molecules, hydronium ions, and hydroxide ions are around -13.87, -32.11, and -25.42 kcal mol^{-1}, respectively, which are little compared to the values of Cr(VI) ions on the NiCo-Ph surface in different media, revealing the stronger adsorption of Cr(VI) ions than other ions, which supports the exchanging of water molecules, hydronium ions, and hydroxide ions for Cr(VI) ions. Therefore, the Cr(VI) ions are decisively adsorbed on the NiCo-Ph surface; this is affirmed by experimental and theoretical studies collectively.
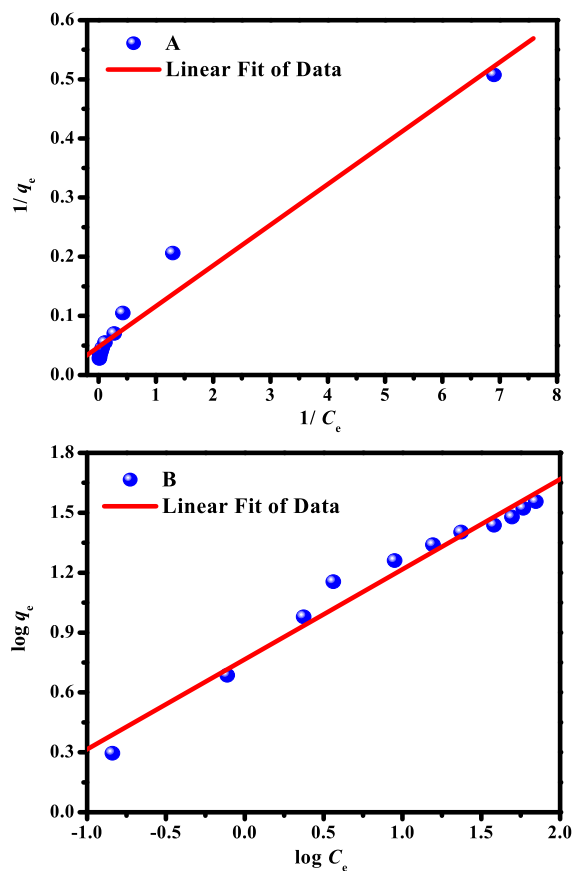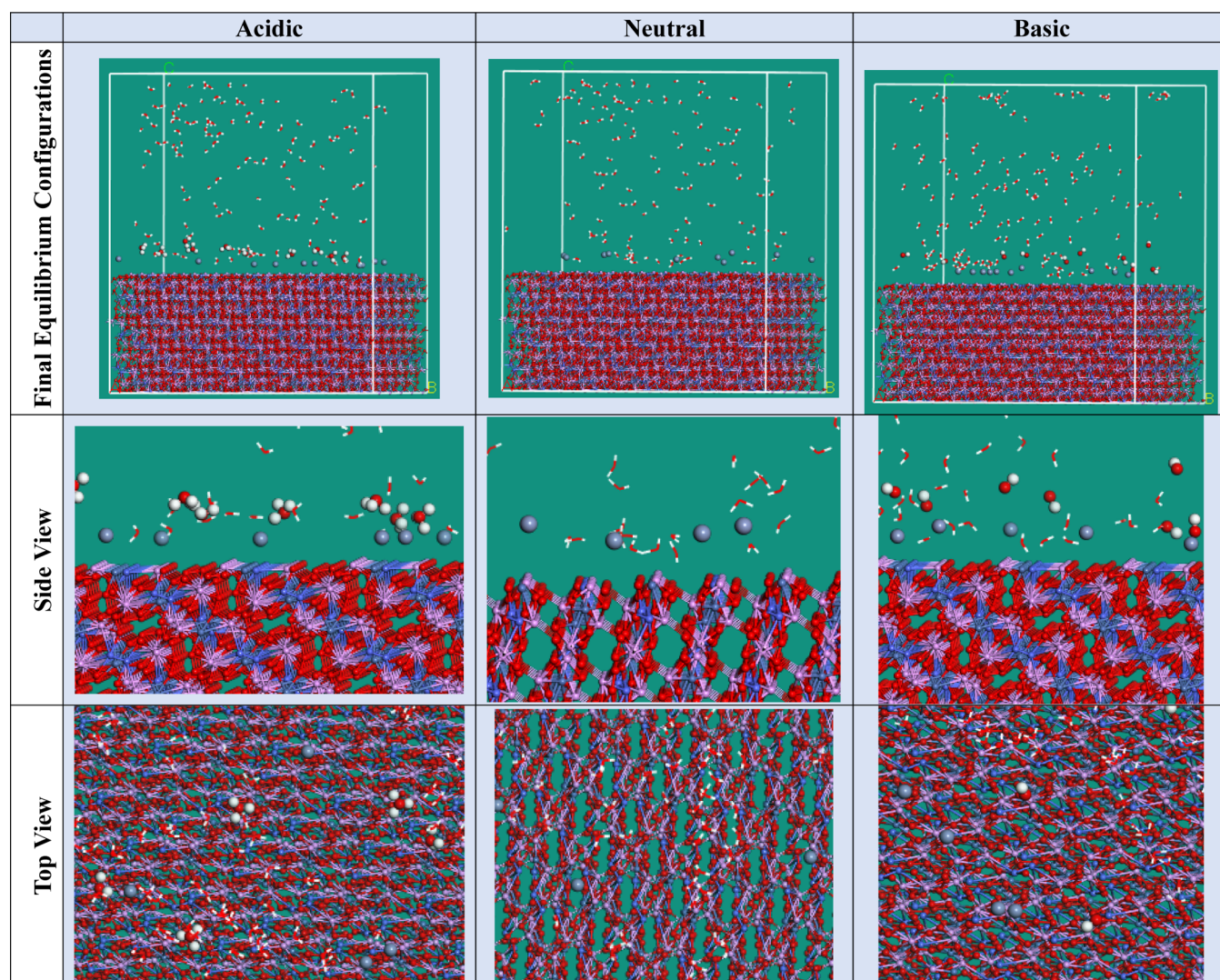
Figure 10. The most suitable configuration for adsorption of Cr(VI) ions on the NiCo-Ph surface in different media obtained using the adsorption locator module.

Table 3. Data and Descriptors Calculated by the MC Simulation for Adsorption of Cr(VI) Ions on the NiCo-Ph Surface in Different Media Obtained by the Adsorption Locator Module

structures	adsorption energy/kcal mol^{-1}	rigid adsorption energy/kcal mol^{-1}	deformation energy/kcal mol^{-1}	dE_{ads}/dN_i: Cr (VI) kcal mol^{-1}	dE_{ads}/dN_i: hydronium kcal mol^{-1}	dE_{ads}/dN_i/ water kcal mol^{-1}	dE_{ads}/dN_i: hydroxide kcal mol^{-1}
NiCo-Ph Cr(IV) water hydronium	−911.62	−822.88	−88.7379	−168.59	−32.11	−14.69	
NiCo-Ph Cr(IV) water	−308.35	−238.51	−69.84	−81.70		−13.40	
NiCo-Ph Cr(IV) water hydroxide	−541.28	−466.12	−75.16	−98.34		13.52	−25.42

3.5. Comparison of the Adsorption Capacity and pH of Solution for Cr(VI) Removal for Some Reported Adsorbents. A comparative study of the investigated NiCo-Ph sorbent with other reported adsorbents is hard because of the variable experimental circumstances related to every study. Table 4 displays the findings of a comparison of the adsorption capacity and pH of solution for Cr(VI) removal for some reported adsorbents.[55−62] The adsorption capacity, q_m (mg/g), was found to be 37.0 mg/g for the fabricated NiCo-Ph. This outcome indicates that this material displays a very significant adsorption capability compared to other kinds of composites

and materials, for instance, nano-Al_2O_3 has a q_m of 17.7 mg/g[55] and hydrous stannic oxide has a q_m of 17.7 mg/g,[56] as recorded in Table 4.

4. CONCLUSIONS

In the present study, the structural and adsorptive characteristics of 2D multilayer nanoflakes of NiCo-Ph for chromium-(VI) removal were thoroughly scrutinized. The bimetal NiCo-Ph was simply manufactured by a sol−gel route in an aqueous solution of HDPCl with the regular addition of a urea-stabilizing agent. In addition, the synthesized NiCo-Ph was

Table 4. Comparison of Adsorption Capacity and pH of Solution for Cr(VI) Removal for Diverse Adsorbents

sorbents	optimum pH	sorbent/solution ratio (g/L)	adsorption capacity q_m (mg/g)	references
nano-Al_2O_3	4	5	17.7	55
hydrous stannic oxide	2	4	3.48	56
treated sawdust of sal tree	3.5	0.1	9.55	57
Dictyopteris polypodioides	1	10	21.78	58
banana peel	2		10.42	59
henna leaves	4		0.078	60
banana peel powder	3		7.35	61
modified groundnut hull	2		31	62
NiCo-Ph	6	5	37.0	this study

fully characterized via various methods including XRD, FTIR, DLS, XPS, SEM, TEM, and studying the nitrogen adsorption–desorption isotherms. SEM and TEM characterizations asserted the self-assembly of the nanoflake structure resulting in the formation of NiCo-Ph flowers with diameters ranging from 20 to 80 nm. XRD and SAED outcomes emphasized the formation of the (020) plane of Co 2p and Ni 2p with a lattice gap (d-spacing) of 6.5 Å related to $Ni_3(PO_4)_2 \cdot xH_2O$ and $Co_3(PO_4)_2 \cdot xH_2O$, respectively. Besides, XPS results proclaim the following oxidation states for NiCo-Ph: Ni^{2+}, PO_4^{3-}, and Co^{3+}. To correlate NiCo-Ph and its adsorbtion potential for the Cr(VI) removal, six control experiments were carried out to identify the optimum parameters. Batch adsorption tests were carried out at room temperature, pH = 6, a sorption time of 60 min, 0.5 g of sorbent per 100 mL of Cr(VI) ions (100 mg/L), and a rate of 300 rpm, which afforded a removal ratio of 92% and an adsorption capacity (q_m) of 37 mg/g. Significantly, NiCo-Ph displayed pronounced adsorption of Cr(VI) throughout the regeneration tests by maintaining ~80% of its intrinsic efficacy even after the 7th adsorption cycle. Raman spectroscopy analysis established the stability of the synthesized adsorbent NiCo-Ph and further asserted its effectiveness for the remediation of water from Cr(VI) ions and their perfect reduction to the Cr(III) state. Likewise, MC simulations also affirmed the facile action of our adsorbent based on the highest proper adsorption configurations for the Cr(VI) ions on the NiCo-Ph surface. Furthermore, the higher negative adsorption energy values of Cr(VI) in the acidic medium of unrelaxed and relaxed adsorbate molecules of −822.88 and −88.7379 kcal mol^{-1}, respectively, emphasize the reasonable adsorption of Cr(VI) ions in acidic medium. Given the above, the bimetal phosphate NiCo-Ph nanoflakes are considered among the most promising adsorbents for Cr(VI) species uptake in a slightly acidic medium and at ambient temperature.

■ AUTHOR INFORMATION

Corresponding Authors

Mai M. Khalaf − *Department of Chemistry, College of Science, King Faisal University, Al-Ahsa 31982, Saudi Arabia; Department of Chemistry, Faculty of Science, Sohag University, Sohag 82524, Egypt*; Email: mmkali@kfu.edu.sa

Mohamed Gouda − *Department of Chemistry, College of Science, King Faisal University, Al-Ahsa 31982, Saudi Arabia*; Email: mgoudaam@kfu.edu.sa

Hany M. Abd El-Lateef − *Department of Chemistry, College of Science, King Faisal University, Al-Ahsa 31982, Saudi Arabia; Department of Chemistry, Faculty of Science, Sohag University, Sohag 82524, Egypt;* orcid.org/0000-0002-6610-393X; Email: hmahmed@kfu.edu.sa

Authors

Kamal Shalabi − *Department of Chemistry, Faculty of Science, Mansoura University, Mansoura 35516, Egypt*

Saad Shaaban − *Department of Chemistry, College of Science, King Faisal University, Al-Ahsa 31982, Saudi Arabia; Department of Chemistry, Faculty of Science, Mansoura University, Mansoura 35516, Egypt*

Complete contact information is available at:
https://pubs.acs.org/10.1021/acsomega.2c00529

Author Contributions

M.M.K. contributed in conceptualization, investigation, methodology, resources, formal analysis, data curation, funding acquisition, writing—original draft, and writing—review and editing. M.G. contributed in investigation, supervision, methodology, resources, formal analysis, data curation, funding acquisition, writing—original draft, and writing—review and editing. K.S. contributed in methodology, resources, data curation, writing—original draft, and writing—review and editing. S.S contributed in data curation, writing—original draft, and writing—review and editing. H.M.A.E.-L. contributed in conceptualization, supervision, investigation, methodology, resources, formal analysis, data curation, funding acquisition, writing—original draft, and writing—review and editing.

Notes

The authors declare no competing financial interest.

■ REFERENCES

(1) Ghorai, S.; Sarkar, A. K.; Pal, S. Rapid Adsorptive Removal of Toxic Pb 2+ Ion from Aqueous Solution Using Recyclable, Biodegradable Nanocomposite Derived from Templated Partially Hydrolyzed Xanthan Gum and Nanosilica. *Bioresour. Technol.* **2014**, *170*, 578−582.

(2) Wang, L. K.; Vaccari, D. A.; Li, Y.; Shammas, N. K. Chemical Precipitation. *Physicochemical Treatment Processes*; Humana Press, 2005; pp 141−197. DOI: 10.1385/1-59259-820-x:141

(3) Tzanetakis, N.; Taama, W. M.; Scott, K.; Jachuck, R. J. J.; Slade, R. S.; Varcoe, J. Comparative Performance of Ion Exchange Membranes for Electrodialysis of Nickel and Cobalt. *Sep. Purif. Technol.* **2003**, *30*, 113−127.

(4) Al-Qodah, Z.; Al-Shannag, M. Heavy Metal Ions Removal from Wastewater Using Electrocoagulation Processes: A Comprehensive Review. *Sep. Sci. Technol.* **2017**, *52*, 2649.

(5) Juang, R.-S.; Shiau, R.-C. Metal Removal from Aqueous Solutions Using Chitosan-Enhanced Membrane Filtration. *J. Membr. Sci.* **2000**, *165*, 159−167.

(6) Sousa, F. W.; Oliveira, A. G.; Ribeiro, J. P.; Rosa, M. F.; Keukeleire, D.; Nascimento, R. F. Green Coconut Shells Applied as

Adsorbent for Removal of Toxic Metal Ions Using Fixed-Bed Column Technology. *J. Environ. Manage.* **2010**, *91*, 1634−1640.

(7) Barakat, M. Removal of Toxic Cyanide and Cu(II) Ions from Water by Illuminated TiO2 Catalyst. *Appl. Catal., B* **2004**, *53*, 13−20.

(8) Barakat, M. A. New Trends in Removing Heavy Metals from Industrial Wastewater. *Arabian J. Chem.* **2011**, *4*, 361−377.

(9) Xu, P.; Cao, J.; Yin, C.; Wang, L.; Wu, L. Quantum Chemical Study on the Adsorption of Megazol Drug on the Pristine BC3 Nanosheet. *Supramol. Chem.* **2021**, *33*, 63−69.

(10) Shamsi, A.; Hashemian, S. Nano Spinels of Copper-Doped Cobalt Aluminate (CoxCu(1-x)Al2O4) for Removal of Cd(II) from Aqueous Solutions. *Desalin. Water Treat.* **2020**, *181*, 346−354.

(11) Meunier, N.; Drogui, P.; Montané, C.; Hausler, R.; Mercier, G.; Blais, J.-F. Comparison between Electrocoagulation and Chemical Precipitation for Metals Removal from Acidic Soil Leachate. *J. Hazard. Mater.* **2006**, *137*, 581−590.

(12) Ropars, M.; Marchal, R.; Pourquié, J.; Vandecasteele, J. P. Large-Scale Enzymatic Hydrolysis of Agricultural Lignocellulosic Biomass. Part 1: Pretreatment Procedures. *Bioresour. Technol.* **1992**, *42*, 197−204.

(13) Rahmani, K.; Mahvi, A. H.; Vaezi, F.; Mesdaghinia, A.; Nabizade, R.; Nazmara, S. N. Bioremoval of Lead by Use of Waste Activated Sludge. *Int. J. Environ. Res.* **2009**, *3*, 471−476.

(14) Yusuff, A. S. Optimization of Adsorption of Cr(VI) from Aqueous Solution by Leucaena Leucocephala Seed Shell Activated Carbon Using Design of Experiment. *Appl. Water Sci.* **2018**, *8*, 232.

(15) Miao, M.-s.; Wang, Y.-n.; Kong, Q.; Shu, L. Adsorption Kinetics and Optimum Conditions for Cr(VI) Removal by Activated Carbon Prepared from Luffa Sponge. *Desalin. Water Treat.* **2015**, *57*, 7763−7772.

(16) Zhang, R.; Ma, H.; Wang, B. Removal of Chromium(VI) from Aqueous Solutions Using Polyaniline Doped with Sulfuric Acid. *Ind. Eng. Chem. Res.* **2010**, *49*, 9998−10004.

(17) Linnikov, O.; Rodina, I.; Shevchenko, V.; Medvedeva, I.; Uimin, M.; Schegoleva, N.; Yermakov, A.; Platonov, V.; Osipov, V. Removal of Cr(VI) from Aqueous Solutions by Magnetite Nanoparticles with Different Sizes and Crystal Structure. *Desalin. Water Treat.* **2013**, *52*, 324−330.

(18) Yadav, S. K.; Dixit, A. K. Efficient Removal of Cr(VI) from Aqueous Solution onto Palm TrunkCharcoal: Kinetic and Equilibrium Studies. *Chem. Sci. J.* **2015**, *7*, 114.

(19) Jhung, S. H.; Yoon, J. W.; Hwang, Y. K.; Chang, J.-S. Morphology Control of the Nanoporous Nickel Phosphate VSB-5 from Large Crystals to Nanocrystals. *Microporous Mesoporous Mater.* **2006**, *89*, 9−15.

(20) Logar, N. Z.; Kaučič, V. Nanoporous Materials: From Catalysis and Hydrogen Storage to Wastewater Treatment. *Acta Chim.* **2006**, *53*, 117−135.

(21) Ramana, C. V.; Ait-Salah, A.; Utsunomiya, S.; Becker, U.; Mauger, A.; Gendron, F.; Julien, C. M. Structural Characteristics of Lithium Nickel Phosphate Studied Using Analytical Electron Microscopy and Raman Spectroscopy. *Chem. Mater.* **2006**, *18*, 3788−3794.

(22) Zhu, Y.-P.; Liu, Y.-L.; Ren, T.-Z.; Yuan, Z.-Y. Mesoporous Nickel Phosphate/Phosphonate Hybrid Microspheres with Excellent Performance for Adsorption and Catalysis. *RSC Adv.* **2014**, *4*, 16018−16021.

(23) Al-Omair, M. A.; Touny, A. H.; Al-Odail, F. A.; Saleh, M. M. Electrocatalytic Oxidation of Glucose at Nickel Phosphate Nano/Micro Particles Modified Electrode. *Electrocatalysis* **2017**, *8*, 340−350.

(24) Tang, Y.; Liu, Z.; Guo, W.; Chen, T.; Qiao, Y.; Mu, S.; Zhao, Y.; Gao, F. Honeycomb-like Mesoporous Cobalt Nickel Phosphate Nanospheres as Novel Materials for High Performance Supercapacitor. *Electrochim. Acta* **2016**, *190*, 118−125.

(25) Alnajjar, A. O.; Abd El-Lateef, H. M.; Khalaf, M. M.; Mohamed, I. M. A. Steel Protection in Acidified 3.5% NaCl by Novel Hybrid Composite of CoCrO3/Polyaniline: Chemical Fabrication, Physicochemical Properties, and Corrosion Inhibition Performance. *Constr. Build. Mater.* **2022**, *317*, 125918.

(26) Gao, G.; Liang, C. Electrochemical and DFT Studies of β-Amino-Alcohols as Corrosion Inhibitors for Brass. *Electrochim. Acta* **2007**, *52*, 4554−4559.

(27) Abd El-Lateef, H. M.; Shalabi, K.; Abdelhamid, A. A. One-Pot Synthesis of Novel Triphenyl Hexyl Imidazole Derivatives Catalyzed by Ionic Liquid for Acid Corrosion Inhibition of C1018 Steel: Experimental and Computational Perspectives. *J. Mol. Liq.* **2021**, *334*, 116081.

(28) Eid, A. M.; Shaaban, S.; Shalabi, K. Tetrazole-Based Organoselenium Bi-Functionalized Corrosion Inhibitors during Oil Well Acidizing: Experimental, Computational Studies, and SRB Bioassay. *J. Mol. Liq.* **2020**, *298*, 111980.

(29) Nie, S.; Zhang, C.; Peng, C.; Wang, D.-y.; Ding, D.; He, Q. Study of the Synergistic Effect of Nanoporous Nickel Phosphates on Novel Intumescent Flame Retardant Polypropylene Composites. *J. Spectrosc.* **2015**, *2015*, 1−7.

(30) Khalaf, M. M.; Abd El-Lateef, H. M.; Touny, A. H.; Saleh, M. M.; Mohamed, I. M. A. Electrocatalytic Performance of Inorganic Nanoflakes Nickel Phosphates under Adjusted Synthetic Parameters towards Urea and Methanol Oxidation in Alkaline Media. *Microchem. J.* **2021**, *163*, 105901.

(31) Amorim, I.; Xu, J.; Zhang, N.; Xiong, D.; Thalluri, S. M.; Thomas, R.; Sousa, J. P. S.; Araújo, A.; Li, H.; Liu, L. Bi-Metallic Cobalt-Nickel Phosphide Nanowires for Electrocatalysis of the Oxygen and Hydrogen Evolution Reactions. *Catal. Today* **2020**, *358*, 196−202.

(32) Jiang, P.; Liu, Q.; Ge, C.; Cui, W.; Pu, Z.; Asiri, A. M.; Sun, X. CoP Nanostructures with Different Morphologies: Synthesis, Characterization and a Study of Their Electrocatalytic Performance toward the Hydrogen Evolution Reaction. *J. Mater. Chem. A* **2014**, *2*, 14634.

(33) Liang, H.; Gandi, A. N.; Anjum, D. H.; Wang, X.; Schwingenschlögl, U.; Alshareef, H. N. Plasma-Assisted Synthesis of NiCoP for Efficient Overall Water Splitting. *Nano Lett.* **2016**, *16*, 7718−7725.

(34) Huang, H.; Yu, C.; Yang, J.; Zhao, C.; Han, X.; Liu, Z.; Qiu, J. Strongly Coupled Architectures of Cobalt Phosphide Nanoparticles Assembled on Graphene as Bifunctional Electrocatalysts for Water Splitting. *ChemElectroChem* **2016**, *3*, 719−725.

(35) Yang, X.; Lu, A.-Y.; Zhu, Y.; Hedhili, M. N.; Min, S.; Huang, K.-W.; Han, Y.; Li, L.-J. CoP Nanosheet Assembly Grown on Carbon Cloth: A Highly Efficient Electrocatalyst for Hydrogen Generation. *Nano Energy* **2015**, *15*, 634−641.

(36) Shao, H.; Padmanathan, N.; McNulty, D.; O'Dwyer, C.; Razeeb, K. M. Supercapattery Based on Binder-Free Co3(PO4)2·8H2O Multilayer Nano/Microflakes on Nickel Foam. *ACS Appl. Mater. Interfaces* **2016**, *8*, 28592−28598.

(37) Suresh Kumar, P.; Korving, L.; Keesman, K. J.; van Loosdrecht, M. C. M.; Witkamp, G.-J. Effect of Pore Size Distribution and Particle Size of Porous Metal Oxides on Phosphate Adsorption Capacity and Kinetics. *Chem. Eng. J.* **2019**, *358*, 160−169.

(38) Khalaf, M. M.; Al-Amer, K.; Abd El-lateef, H. M. Magnetic Fe$_3$O$_4$ Nanocubes Coated by SiO$_2$ and TiO$_2$ Layers as Nanocomposites for Cr (VI) up Taking from Wastewater. *Ceram. Int.* **2019**, *45*, 23548−23560.

(39) Timbo, C. C.; Kandawa-Schulz, M.; Amuanyena, M.; Kwaambwa, H. M. Adsorptive Removal from Aqueous Solution of Cr(VI) by Green Moringa Tea Leaves Biomass. *J. Encapsulation Adsorpt. Sci.* **2017**, *7*, 108−119.

(40) Recillas, S.; Rodríguez-Lugo, V.; Montero, M. L.; Viquez-Cano, S.; Hernandez, L.; Castaño, V. M. Studies on the Precipitation Behavior of Calcium Phosphate Solutions. *J. Ceram. Process. Res.* **2012**, *13*, 5−10.

(41) Granados, C. F.; Serrano, G. J.; Bonifacio, M. J. Synthesis and Characterization of Inorganic Materials to Be Employees as Adsorbents of Toxic Metals. *Sintesis y caracterizacion de materiales inorganicos para ser empleados como adsorbentes de metales toxicos y de interes nuclear*; Instituto Nacional de Investigaciones Nucleares: Mexico, 2010.

(42) Honciuc, A. Surfactants and Amphiphiles. *Chemistry of Functional Materials Surfaces and Interfaces*; Elsevier, 2021; pp 43−77.

(43) Shi, C.; Wu, Z.; Yang, F.; Tang, Y. Janus Particles with PH Switchable Properties for High-Efficiency Adsorption of PPCPs in Water. *Solid State Sci.* 2021, *119*, 106702.

(44) Agbe, H.; Raza, N.; Dodoo-Arhin, D.; Chauhan, A.; Kumar, R. V. H(2)O(2) Rejuvenation-Mediated Synthesis of Stable Mixed-Morphology Ag(3)PO(4) Photocatalysts. *Heliyon* 2018, *4*, No. e00599.

(45) Yadav, A. K.; Singh, P. A Review of the Structures of Oxide Glasses by Raman Spectroscopy. *RSC Adv.* 2015, *5*, 67583−67609.

(46) Litasov, K. D.; Podgornykh, N. M. Raman Spectroscopy of Various Phosphate Minerals and Occurrence of Tuite in the Elga IIE Iron Meteorite. *J. Raman Spectrosc.* 2017, *48*, 1518−1527.

(47) Karthik, C.; Ramkumar, V. S.; Pugazhendhi, A.; Gopalakrishnan, K.; Arulselvi, P. I. Biosorption and Biotransformation of Cr(VI) by Novel Cellulosimicrobium Funkei Strain AR6. *J. Taiwan Inst. Chem. Eng.* 2017, *70*, 282−290.

(48) Tan, J.; Song, Y.; Huang, X.; Zhou, L. Facile Functionalization of Natural Peach Gum Polysaccharide with Multiple Amine Groups for Highly Efficient Removal of Toxic Hexavalent Chromium (Cr(VI)) Ions from Water. *ACS Omega* 2018, *3*, 17309−17318.

(49) Zhou, L.; Duan, Y.; Xu, X. Facile Preparation of Amine-Rich Polyamidoamine (PAMAM) Gel for Highly Efficient Removal of Cr(VI) Ions. *Colloids Surf., A* 2019, *579*, 123685.

(50) Qiu, B.; Wang, Y.; Sun, D.; Wang, Q.; Zhang, X.; Weeks, B. L.; O'Connor, R.; Huang, X.; Wei, S.; Guo, Z. Cr(vi) Removal by Magnetic Carbon Nanocomposites Derived from Cellulose at Different Carbonization Temperatures. *J. Mater. Chem. A* 2015, *3*, 9817−9825.

(51) Zhou, Y.; Yang, M.; Wu, W.; Vasiliev, A. L.; Zhu, K.; Padture, N. P. Room-Temperature Crystallization of Hybrid-Perovskite Thin Films via Solvent−Solvent Extraction for High-Performance Solar Cells. *J. Mater. Chem. A* 2015, *3*, 8178−8184.

(52) El-Katori, E. E.; Nessim, M. I.; Deyab, M. A.; Shalabi, K. Electrochemical, XPS and Theoretical Examination on the Corrosion Inhibition Efficacy of Stainless Steel via Novel Imidazolium Ionic Liquids in Acidic Solution. *J. Mol. Liq.* 2021, *337*, 116467.

(53) Özcan, M.; Dehri, I.; Erbil, M. Organic Sulphur-Containing Compounds as Corrosion Inhibitors for Mild Steel in Acidic Media: Correlation between Inhibition Efficiency and Chemical Structure. *Appl. Surf. Sci.* 2004, *236*, 155−164.

(54) Dehghani, A.; Mostafatabar, A. H.; Bahlakeh, G.; Ramezanzadeh, B. A Detailed Study on the Synergistic Corrosion Inhibition Impact of the Quercetin Molecules and Trivalent Europium Salt on Mild Steel; Electrochemical/Surface Studies, DFT Modeling, and MC/MD Computer Simulation. *J. Mol. Liq.* 2020, *316*, 113914.

(55) Yin, J.; Jiang, Z.; Chang, G.; Hu, B. Simultaneous On-Line Preconcentration and Determination of Trace Metals in Environmental Samples by Flow Injection Combined with Inductively Coupled Plasma Mass Spectrometry Using a Nanometer-Sized Alumina Packed Micro-Column. *Anal. Chim. Acta* 2005, *540*, 333−339.

(56) Ghosh, U. C.; Goswami, S. Studies on Adsorption Behaviour of Cr(VI) onto Synthetic Hydrous Stannic Oxide. *Water SA* 2006, *31*, 597−602. DOI: 10.4314/wsa.v31i4.5150.

(57) Baral, S. S.; Das, S. N.; Rath, P. Hexavalent Chromium Removal from Aqueous Solution by Adsorption on Treated Sawdust. *Biochem. Eng. J.* 2006, *31*, 216−222.

(58) Sabour, B.; Belattmani, Z.; Tahiri, S.; Zrid, R.; Reani, A.; Elatouani, S.; Loukili, H.; Hassouani, M.; Krati, M. E.; Bentiss, F. Bioremoval of Hexavalent Chromium from Aqueous Solutions by the Brown Seaweed Dictyopteris Polypodioides. *Res. J. Environ. Toxicol.* 2015, *9*, 218−230.

(59) Parlayici, Ş.; Pehlivan, E. Comparative Study of Cr(VI) Removal by Bio-Waste Adsorbents: Equilibrium, Kinetics, and Thermodynamic. *J. Anal. Sci. Technol.* 2019, *10*, 15.

(60) Shanthi, T.; Selvarajan, V. M. Removal of Cr(VI) and Cu(II) Ions from Aqueous Solution by Carbon Prepared from Henna Leaves. *J. Chem.* 2013, *2013*, 1−6.

(61) Badessa, T. S.; Wakuma, E.; Yimer, A. M. Bio-Sorption for Effective Removal of Chromium(VI) from Wastewater Using Moringa Stenopetala Seed Powder (MSSP) and Banana Peel Powder (BPP). *BMC Chem.* 2020, *14*, 71.

(62) Owalude, S. O.; Tella, A. C. Removal of Hexavalent Chromium from Aqueous Solutions by Adsorption on Modified Groundnut Hull. *Beni-Suef Univ. J. Basic Appl. Sci.* 2016, *5*, 377−388.